PHYSICAL ELECTRONICS

Highly Efficient Gyrotron with Multi-Stage Recuperation of Residual Electron Energy

O. I. Louksha[a],* and P. A. Trofimov[a]

[a] Peter the Great St. Petersburg Polytechnic University, St. Petersburg, 195251 Russia
*e-mail: louksha@rphf.spbstu.ru
Received April 30, 2019; revised April 30, 2019; accepted May 21, 2019

Abstract—The results of complex modeling of physical processes in a gyrotron of moderate power in the 4-mm wavelength range have been presented. Methods for improving the quality of the helical electron beam and gyrotron electronic efficiency based on the optimization of the electric field distribution in the cathode region have been implemented. The design of a collector with four-stage recuperation of residual beam energy based on the method of spatial separation of electrons in crossed azimuthal magnetic and axial electric fields has been developed. A gyrotron total efficiency equal to 71.8% has been achieved by improving the quality of the electron beam and efficient energy recuperation in the collector region.

INTRODUCTION

Currently, gyrotrons occupy a leading position among the sources of powerful microwave radiation in the millimeter and submillimeter wavelength ranges. Gyrotrons of megawatt power operating at long-pulse and quasi-continuous regimes are in demand for heating dense plasma and current control in controlled fusion installations. These devices are also used in the processing of materials, in high-resolution spectroscopy, to diagnose different media, and other applications.

The efficiency of interaction of the helical electron beam (HEB) with a high-frequency field in the gyrotron resonator is relatively low. As a rule, the electronic efficiency of powerful gyrotrons does not exceed 30−35% [1−3]. An efficiency improvement can be achieved by the optimization of the HEB formation system, aimed at creating a high-quality beam with a large pitch factor, low velocity and energy spreads, and a required spatial structure [4]. Pitch factor $\alpha = v_\perp / v_\parallel$ ($v_\perp$ and $v_\parallel$ are the transverse and longitudinal components of the electron velocity) is used to characterize the fraction of the energy concentrated in the transverse motion of electrons from which the energy of the output microwave radiation is "extracted" in gyroresonance devices.

The gyrotrons of megawatt power with frequencies of 110 and 140 GHz and electronic efficiency of more than 40%, manufactured at the Institute of Applied Physics, Russian Academy of Sciences (IAP RAS) [2, 5], can be cited as an example of such optimization. Experimental studies aimed at improving the quality

of HEB were also carried out at Peter the Great St. Petersburg Polytechnic University (SPbPU) using a pulsed gyrotron with an operating frequency of 74.2 GHz and an output power of about 100 kW [6−11]. As a result of these studies, the electronic efficiency of the gyrotron was increased to 46% by optimizing the distributions of electric and magnetic fields in the region of HEB formation, as well as increasing the homogeneity of thermionic emission from the cathode [11].

An increase in the total efficiency of gyrotrons can be achieved as a result of recuperation: return to the electric network of a part of the energy of the electron stream that was not used up in its interaction with a high-frequency field. Almost all modern powerful gyrotrons are equipped with single-stage depressed collectors in which electron deceleration occurs in the gap between the tube body and the collector isolated from it. Such systems can significantly increase the gyrotron total efficiency (up to by 1.5 times compared to the electronic efficiency in the absence of recuperation [1, 2, 12]). It is fundamentally important for powerful long-pulse and quasi-continuous gyrotrons that the thermal load on the collector is also reduced during recuperation of residual electron energy.

A further increase in total efficiency is possible with the use of multistage recuperation systems, which imply the separation of beam fractions with different energies in space and deposition of these fractions on collector sections under different potentials (for example, [13−17]). However, such systems, as far as we know, have not yet been implemented in gyrotron-
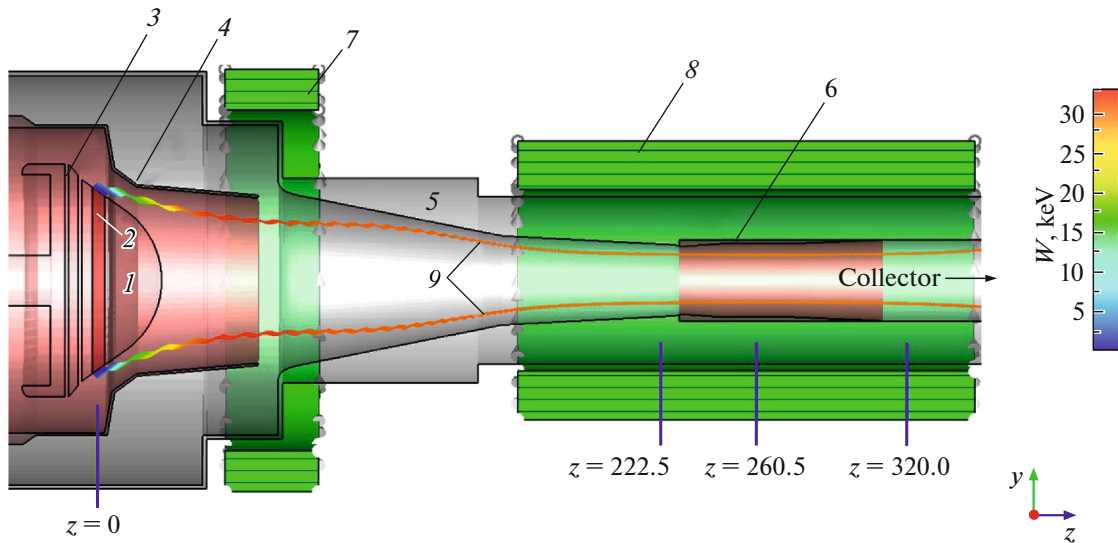
Fig. 1. Schematic representation of the gyrotron model: (*1*) cathode, (*2*) emitting strip, (*3*) control electrode, (*4*) anode, (*5*) device body, (*6*) resonator, (*7*) cathode coil, (*8*) main solenoid, and (*9*) electron trajectories (color of trajectories corresponds to the energy of particles *W*).

type devices in practice. This is due to the specificity of electronic trajectories in the collector region of these devices, the existence of electron spread over the velocity components and coordinates, and the presence of a relatively strong magnetic field. New possibilities for the separation of electrons with different energies are opened by using the approach based on their drift in crossed electric and magnetic fields [18−20]. A multistage recuperator in which electron drift is carried out in azimuthal magnetic and axial electric fields was developed based on this approach at SPbPU [21, 22].

This study presents the results of complex modeling of the processes in the gyrotron made at SPbPU, including the formation of HEB in the electron-optical system (EOS), interaction of electrons with a high-frequency field, and beam transport in the collector region. This study was aimed at achieving record values of the gyrotron total efficiency due to both the formation of high-quality HEB and the effective recuperation of residual energy in a multistage collector system. The calculations were performed using the 3D modeling software package CST Studio Suite [23]. At different stages of modeling, data were compared with the results of experiments performed with this gyrotron.

1. TRAJECTORY ANALYSIS OF HEB IN THE ELECTRON-OPTICAL GYROTRON SYSTEM

The formation of HEB in the gyrotron at SPbPU is performed using a three-electrode magnetron injection gun (MIG) (Fig. 1). The cathode block of the gun includes a control electrode by changing the potential of which the average pitch factor and the velocity

spread of electrons can be changed [9, 24]. The main parameters of the gyrotron are shown in Table 1. Values U_0, I_b, B_0, and B_c given in this table correspond to the calculated operating regime of the gyrotron with an average pitch factor of approximately 1.3. The values of these quantities varied in both calculations described below and the experiments, which allowed changing the beam characteristics at the resonator entrance and the generated microwave power within operating mode $TE_{12,3}$. Self-consistent electronic trajectories were calculated using the Tracking Solver. Two regimes of thermionic emission from the cathode were investigated. In the first regime (homogeneous cathode), emission with the same current density was carried out from the entire emitting strip. In this case, the beam consisted of 3600 electronic trajectories (beamlets). In the second regime (sectioned cathode, 2200 trajectories), there was no emission from the two azimuthal sectors of 70° each the positions of which corresponded to the locations of the "bundles" of toroidal collector solenoid (see Section 3). Electron spread over initial thermal velocities was considered in emission modeling. The full current of HEB was 10 A in both regimes. The distribution of the magnetic field for a given geometry of the coils was determined using the Magnetostatic Solver and then exported to the current project. The calculation model in the trajectory analysis was divided into about 80×10^6 cells.

The average radius of the hollow HEB in the resonator and, as a consequence, the output microwave power can be adjusted by changing magnetic compression value B_0/B_c. In these calculations, the value of B_0/B_c was changed by the variation in the number of turns of the cathode coil [6]. The maximum output

power values were obtained at $B_0/B_c = 17.01$, which corresponds to 26 turns of the coil. The regime with minimum velocity spread $\delta v_\perp$ and average pitch-factor α in the range of 1.5–1.6 (the potentials of cathode $U_c = -30$ kV and device body $U_{body} = 0$ were not changed) was chosen by the variation of the potentials of anode U_a and control electrode U_{cont} at given B_0/B_c. Here and further in Section 1, the values of HEB parameters refer to the central plane of resonator $z = 260.5$ mm (Fig. 1). Note that the maximum gyrotron efficiency was achieved earlier in experiments at a calculated value of α equal to about 1.6 [11].

The following values of HEB parameters were obtained at $B_0/B_c = 17.01$, $U_a = 8.4$ kV, and $U_{cont} = -44.5$ kV: $\alpha = 1.57$, $\delta v_\perp = 2.8\%$ for a homogeneous cathode and $\alpha = 1.52$, $\delta v_\perp = 3.4\%$ for the sectioned one. The $\delta v_\perp$ value was determined as the standard deviation from the mean transverse velocity. The particle distribution in the HEB cross-sectional plane for both cathodes is shown in Fig. 2. Inhomogeneous emission from the cathode is one of the factors impairing the quality of HEB (for example, [24]). Therefore, the transition from a homogeneous to a sectioned cathode increases the spread of electrons in velocities and energies and there is an additional displacement of electrons along the radius due to the action of crossed azimuthal electric and longitudinal magnetic fields. A strong magnetic field ensures the preservation of the required electron distribution along the azimuthal coordinate for the sectioned cathode when there are no particles within the two azimuthal sectors.

It is important to note that the additional velocity spread in real conditions can be caused by the action of factors not taken into account in this simulation: the roughness of the cathode emitting surface, imperfec-

Table 1. The main geometric parameters of the gyrotron and the characteristics of its operating regime

Parameter	Value
Accelerating voltage	$U_0 = 30$ kV
Beam current	$I_b = 10$ A
Magnetic field induction in the resonator region	$B_0 = 2.75$ T
Magnetic field induction at the cathode	$B_c = 0.152$ T
Operational mode	$TE_{12,3}$
Operational frequency	$f_0 = 74.2$ GHz
Resonator radius	$R_0 = 14.45$ mm
The average radius of the emitting strip of the cathode	$R_c = 35$ mm

tions of manufacturing and adjustment of tube elements, and high-frequency fields caused by the development of parasitic instabilities (see, for example, [4]). High-frequency fields can also cause, in addition to increasing the velocity spread, a noticeable increase in the energy spread of electrons. Wherein, the cathode surface roughness should be taken into account in the first place if we consider well-designed and adjusted EOS, in which the development of parasitic instabilities is suppressed. The roughness with micron irregularities, typical of modern thermal cathodes, leads to a velocity spread of a few percent [4, 25, 26].

Increasing the velocity spread limits the possibility of increasing the operating pitch factor, since the reflection of electrons from the magnetic mirror and the development of parasitic low-frequency oscillations in the trap between the cathode and the resonator are inevitable at high α and $\delta v_\perp$ (for example, [4, 6, 27, 28]).
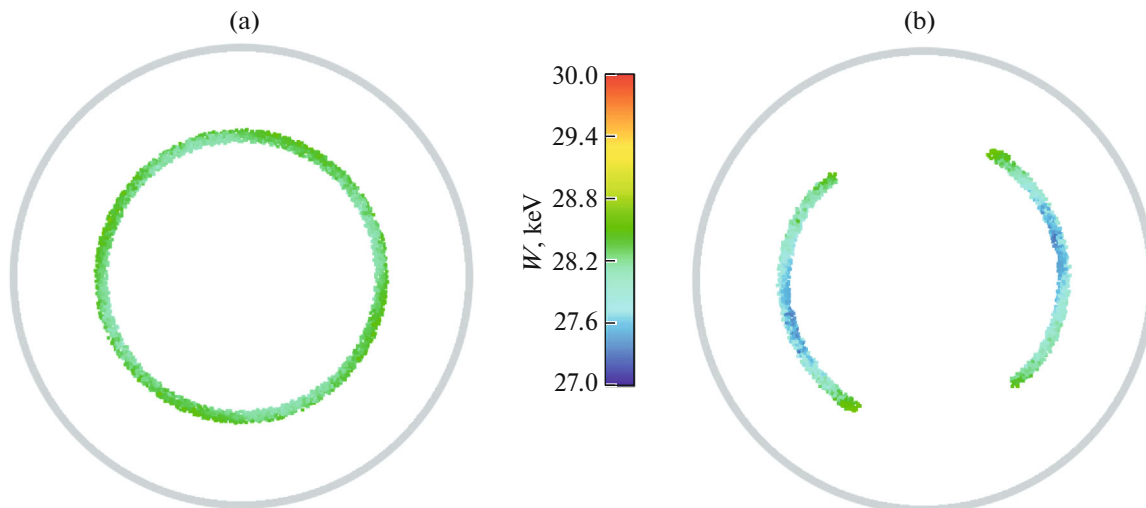

Fig. 2. Particle distributions in the central plane of resonator $z = 260.5$ mm obtained by trajectory analysis of the gyrotron EOS for (a) homogeneous and (b) sectioned cathodes. The color of the particles corresponds to their energy W.
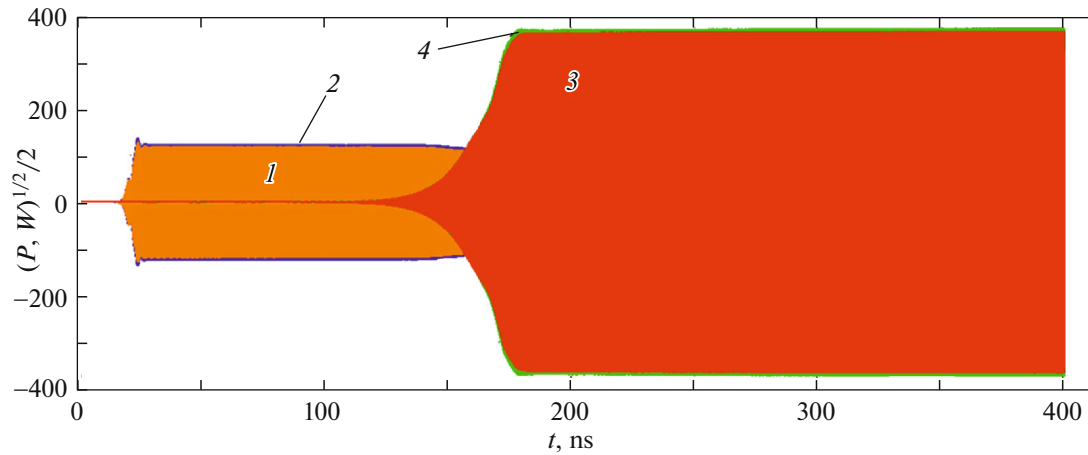
Fig. 3. Time variation of the signals of the (*1, 2*) $TE_{11,3}$ and (*3, 4*) $TE_{12,3}$ modes in the output port of the gyrotron with a homogeneous cathode.

The threshold coefficient of reflection from magnetic mirror R_{th} determined on the basis of the experimental data received at the SPbPU gyrotron, above which these oscillations exist in the electronic space charge, was approximately 1.7×10^{-3} [10]. The specified R_{th} value at Gaussian velocity distribution is achieved when $\alpha = 1.57$ and $\delta v_\perp = 6.3\%$ or when $\alpha = 1.52$ and $\delta v_\perp = 6.7\%$. In the experiment, maximum gyrotron efficiency $\eta_{el} = 46\%$ was obtained at a calculated pitch factor of ~1.6 and a small velocity spread when parasitic low-frequency oscillations were not recorded [11]. This gives grounds to assert that the regimes studied in this paper with pitch factor $\alpha = 1.5-1.6$ can also be implemented in the absence of electron reflection from the magnetic mirror.

The data on the HEB parameters obtained in the trajectory analysis of the gyrotron EOS were used at the second stage in modeling the interaction of electrons with a high-frequency field in the resonator. For this, a special Particle Export Interface monitor, which was the source of particles in the calculations described in the next section, was installed in the plane $z = 222.5$ mm (Fig. 1).

2. MODELING OF PROCESSES IN THE GYROTRON RESONATOR

The design of the SPbPU gyrotron electrodynamic system was performed previously by researchers at IAP RAS. A resonator with a radius of 14.45 mm and a regular part length of 28 mm (Fig. 1) was designed for operating mode $TE_{12,3}$.

The preliminary calculations made it possible to determine the eigenmodes of the resonator, as well as the optimal values of the HEB average radius and magnetic field induction. The simulation of dynamic processes described below was performed using the Particle-in-Cell (PIC) Solver. In this case, the calcu-

lated area was limited by input plane $z = 222.5$ mm and plane $z = 320$ mm, where the output port registering the generated microwave power was installed (Fig. 1). The calculation model was divided into approximately 6×10^6 cells. The integration time step was ~4×10^{-4} ns.

The average radius of the beam in the central plane of the resonator is approximately 8.5 mm at the optimal value of magnetic compression coefficient $B_0/B_c = 17.01$. The maximum value of the output power in the excitation zone of operating mode $TE_{12,3}$ was recorded at the induction of the magnetic field in resonator $B_0 = 2.747$ T. Figure 3 shows the time variation of the signals of modes with the highest amplitude in the output port, which were obtained for a homogeneous cathode with the HEB parameters specified in Section 2 at $B_0/B_c = 17.01$ and $B_0 = 2.747$ T. The numbers of these modes are determined by the structure of high-frequency electric and magnetic fields. At the initial stage of calculation (up to about 140 ns), parasitic mode $TE_{11,3}$ is generated at a frequency of ~71.4 GHz. Subsequently, this mode is suppressed simultaneously with the excitation of operating mode $TE_{12,3}$. A stable generation with a frequency of ~74.5 GHz is observed during the time of $180 < t < 400$ ns. In both modes, there are two polarization components with approximately the same amplitude (Fig. 3), whose superposition provides circular polarization of the wave in the resonator.

The wave-particle power transfer is $P_{RF} = 141$ kW at $t = 400$ ns and electronic efficiency $\eta_{el} = 47\%$ at $U_0 = 30$ kV and $I_b = 10$ A. Almost all power is concentrated in operating mode $TE_{12,3}$: summing the signals of the two components of this mode gives ~137 kW. The mode excitation pattern does not change fundamentally when working with a sectioned cathode. There is only a slight decrease in the output microwave power, which is due, obviously, to the lower quality of the HEB.
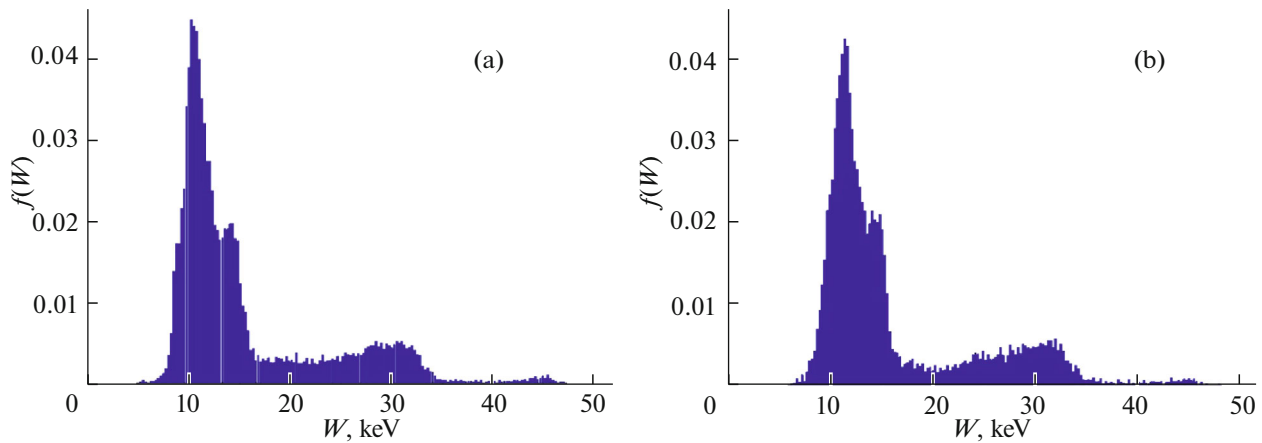
Fig. 4. Histograms of electron energy distribution in the spent HEB for the (a) homogeneous and (b) sectioned cathodes. The electron energy range is divided into 400 intervals.

The total output power for this cathode is ∼138 kW at $t =$ 400 ns and the power in mode $TE_{12,3}$ is 128 kW.

The necessary information for the design of the recuperation system is the data on the parameters of the spent HEB that passed through the resonator and gave part of its energy to the high-frequency field. These data were recorded in the plane of output port $z = 320$ mm. The PIC 2D Monitor for particles, which collected data for a time of $t = 0.003$ ns, was installed here. Each file corresponding to selected time moment t contains information about approximately 25×10^3 particles at this Δt value. Figure 4 shows the energy spectra of electrons in the spent HEB for (a) homogeneous and (b) sectioned cathodes. The values of the potentials of collector sections at which the minimum value of the power dissipated in the form of heat in these sections is provided were chosen based on data on the electron energy distribution [21, 22].

Using the ratio

$$\eta_{el} = 1 - \frac{\int_0^\infty f(W)WdW}{eU_0},$$

from the known energy spectrum $f(W)$, the η_{el} electron efficiency can be estimated. For example, for a homogeneous cathode after the integration of the spectrum shown in Fig. 4a, we obtain $\eta_{el} = 47.9\%$ at a full energy of particles $eU_0 = 30$ keV, which is quite close to the efficiency value determined by the output microwave power.

3. TRAJECTORY ANALYSIS OF THE SPENT HEB IN THE COLLECTOR REGION

The SPbPU gyrotron recuperator uses a method of spatial separation of electrons based on their drift in crossed azimuthal magnetic and axial electric fields [19, 21, 22]. The collector region model is shown in

Fig. 5. The azimuthal magnetic field is created by a solenoid with a toroidal winding. Helmholtz coils are used to correct the distribution of the axial magnetic field along the longitudinal coordinate. The choice of the geometry of the magnetic system ensures adiabatic distribution of the magnetic field in the transition region between the resonator and collector and quasi-homogeneity of this field in the recuperation region with a length of approximately 350 mm. The amplitudes of the axial and azimuthal components of magnetic field induction on the beam radius are approximately 0.04 and 0.08 T in this region.

The electric field is created by four electrode-sections of conical shape, whose potentials decrease as the distance from the resonator increases. The drift in crossed electric and magnetic fields leads to spatial separation of electrons with different energies and their deposition on the sections under different potentials. The collector body is separated from the main body of the gyrotron by a special insulator, which allows implementing a simple one-stage recuperation scheme when the sections and collector body are connected to each other. It also has two connecting tubes, inside of which there are "bundles" (the conductors connecting the turns of the inner winding of the toroidal coil with the turns of its outer winding; see Fig. 5). The magnetic field of the bundles distorts the nearby trajectories of electrons and can lead to their reflection towards the resonator. We used in these studies a sectioned cathode with suppressed emission from two azimuthal sectors of the emitting strip to reduce the negative impact of the bundles. The described collector system was implemented in an experimental gyrotron.

When performing the trajectory analysis of the HEB in the collector region, the possibility of achieving the maximum efficiency of the recuperation of residual energy, i.e., reducing to a minimum the amount of P_{diss} power dissipated as heat during elec-
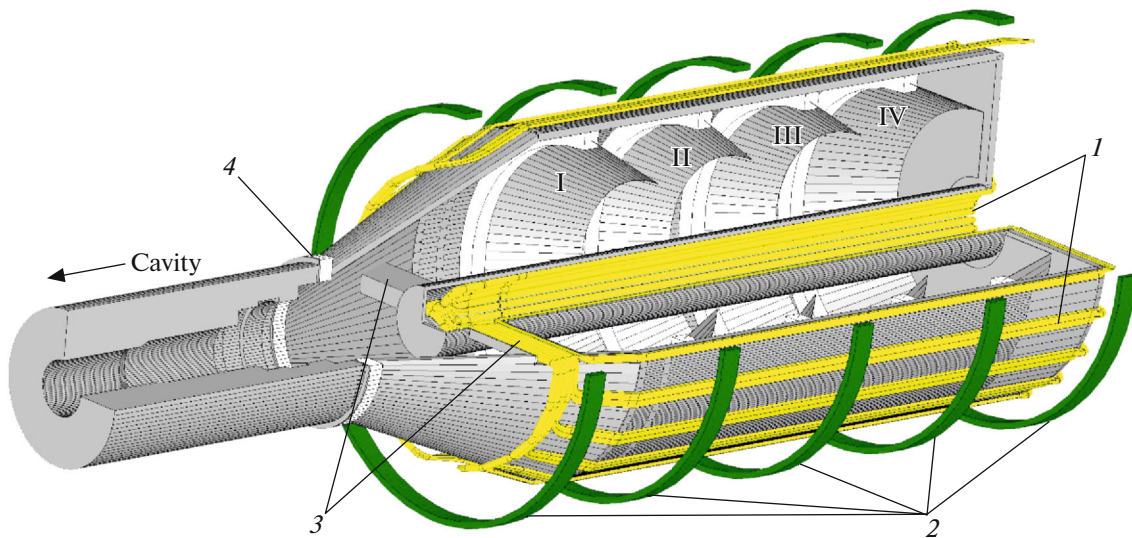
Fig. 5. Schematic representation of the collector model: (*1*) solenoid with toroidal winding, (*2*) Helmholtz coils, (3) "bundles" of wires, (*4*) insulator, and I–IV are the collector sections.

tron deposition on the collector walls, was investigated. Note that the collector was located in the region where the magnetic field induction is significantly less than the B_0 value in the resonator. Therefore, almost all the kinetic energy of electrons is concentrated in their longitudinal (along the magnetic field line) motion. The electron minimum energy W_{min} in the spectrum of the spent HEB (Fig. 4) determines the value of voltage U_I applied to the first section of the collector. The electrons with low energies can change the direction of their longitudinal velocity at $|eU_I| > W_{min}$, i.e., can be reflected towards the resonator. The reflection of electrons with higher energies can also occur in the area between sections. The danger is represented by those electrons that do not deposit on the collector walls after changing the direction of the velocity, but, leaving the collector region and moving in an adiabatically changing magnetic field, reach the resonator. Such electrons can take energy from a high-frequency field interacting with it, which negatively affects the value of the output microwave power. As shown by previous studies, the limit level of reflection from the collector above which the output power falls can vary markedly in different gyrotrons [5, 29–32] and reach about 10% [33].

In the developed scheme of the recuperator with an azimuthal magnetic field, the radial drift leads to the deposition of the main part of the reflected electrons on the back wall of the collector sections, which significantly reduces the flow of particles returning to the resonator [19]. For the same reason, it is practically impossible for secondary electrons to enter the resonator from the bombarded surfaces of collector electrodes.

A multiparameter task to achieve the minimum value of the P_{diss} power by optimization of the geometry and potentials of collector sections and azimuthal position of cathode sectors with suppressed emission at a current of the particles reflected from the collector not exceeding 1–2% of the total HEB current was solved in the present study. As a result of such optimization, the regime in which the P_{diss} power dissipated at the collector was 54.19 kW and the current of the electrons reflected from the collector and passing towards the resonator through input plane $z = 320$ mm was 1.37% of I_b was obtained. In this regime, the collector body was connected with the gyrotron body and sections I–IV of the collector had the following potentials: $U_I = -7.72$ kV, $U_{II} = -10.72$ kV, $U_{III} = -14.72$ kV, and $U_{IV} = -24.72$ kV. The 3D trajectories of electrons in the collector region are shown in Fig. 6. It is seen that the use of a sectioned emitter ensures the passage of electrons to the recuperation region without their deposition on the connecting tubes, in which there are toroidal coil bundles of wires. As electrons move in a decelerating electric field, their energy decreases and they shift to higher radii under the action of crossed $E \times B$ fields.

The position of electronic trajectories in the r–z plane is shown in Fig. 7. The trajectories with different values of energy, pitch factor, and radial coordinate in input plane $z = 320$ mm and passing at approximately equal distance from the bundles were selected (Table 2). The average pitch factor of electrons in the input plane is ~0.59. Since the exchange of energy between the HEB and high-frequency field changes the transverse velocity of electrons, it is obvious that, on average, with increasing energy of particles in the spent beam, their pitch factor also increases. The figure also shows
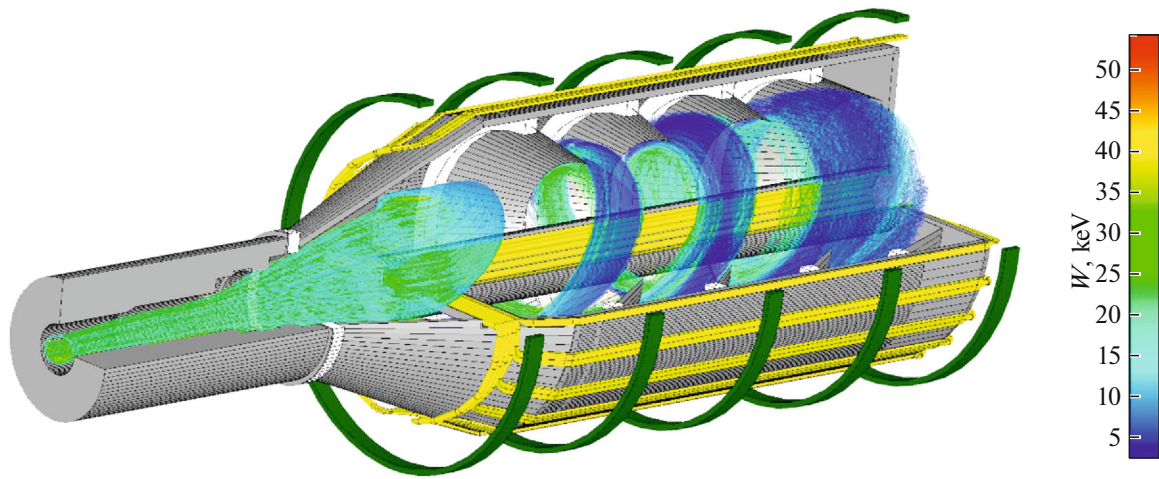
Fig. 6. 3D-trajectories of the electrons in the collector region. The color of the trajectories corresponds to the energy of the particles W.
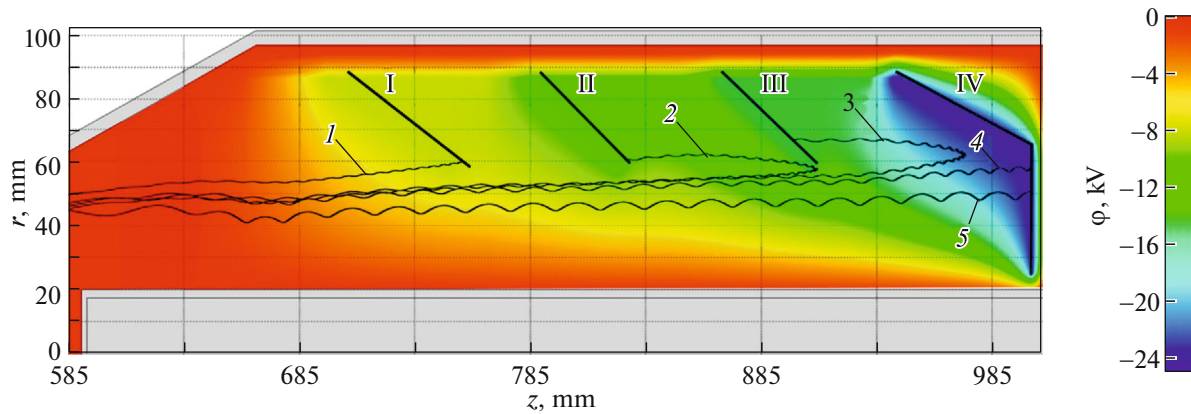

Fig. 7. (*1−5*) Trajectories of the electrons and potential distribution φ in the $r−z$ plane. The elements of the magnetic system and the electrodes shielding I−IV sections from the collector body are not shown.

the potential distribution at the above $U_I−U_{IV}$ values. The presented trajectories demonstrate the correct operation of the method of spatial separation of electrons in crossed $E \times B$ fields, which provides the deposition of particles with different energies on the sections under the corresponding potential.

At the considered regime of gyrotron operation, its total efficiency is

$$\eta_t = \frac{P_{RF}}{P_{RF} + P_{diss}} = 71.8\%,$$

where $P_{RF} = 138$ kW and $P_{diss} = 54.19$ kW. The power dissipated at the collector is distributed over its electrodes in the following way: the power values at sections $P_I = 36.15$ kW, $P_{II} = 4.79$ kW, $P_{III} = 5.24$ kW, and $P_{IV} = 7.58$ kW and the power value on collector body $P_{coll} = 0.43$ kW. The recuperation efficiency is 66.5%. Most electrons are deposited on the first section in this recuperator. This is a consequence of the need to

reduce the radius of the inner aperture of this section and reduce the value of $|eU_I|$ in order to provide a relatively small reflection of electrons towards the resonator. The main causes for the reflection of electrons and their missing the appropriate section are the disturbing influence of the bundles' magnetic field and electron spread in radial coordinates at the recuperator entrance. If the permissible reflection threshold is increased, it is possible to achieve an increase in the

Table 2. Input parameters of electron trajectories

No.	Energy, keV	Pitch factor	Radius, mm
1	8.270	0.45	9.34
2	13.781	0.45	8.7
3	21.264	0.74	9.04
4	28.097	0.83	9.03
5	46.368	1.65	8.63

total efficiency. Note that the maximum total efficiency is 81.2% for the residual energy of electrons when they are deposited on sections $W_{rem} > 0.5$ keV and 83.6% at $W_{rem} > 0$ (at the reflection from the collector equal to 1.37%) for the spectrum of the spent HEB, shown in Fig. 4b, in the case of a four-stage collector with perfect separation, when any of the electrons falls on a section with a potential corresponding to its energy.

The possibilities of further increase of the efficiency of the developed recuperation method are connected, obviously, with improvement of the design of the magnetic system providing the required distribution of the azimuthal magnetic field. The authors continue to search for the optimal way to create such a field, which would increase the total efficiency of gyrotrons, including powerful gyrotrons operating at long-pulse and quasi-continuous regimes.

CONCLUSIONS

Thus, the complex simulation performed in the study showed the possibility of achieving record values of the total efficiency of the pulsed gyrotron of moderate power of 4-mm wavelength, obtained as a result of improving the quality of the HEB in the electron-optical system and recuperation of the residual electron energy in a multistage collector system. The design of a four-stage recuperator based on the method of spatial separation of electrons in crossed azimuthal magnetic and axial electric fields was developed. The use of a sectioned cathode with suppressed emission from two azimuthal sectors can improve recuperation efficiency and reduce the coefficient of the reflection of the electrons from the collector. A total efficiency of 71.8% with a recuperation efficiency of 66.5% and a current of the electrons reflected from the collector amounting to 1.37% of the HEB total current was achieved at the gyrotron operation optimal regime.

FUNDING

CONFLICT OF INTEREST

The authors state that they do not have any conflicts of interest.

REFERENCES

1. A. G. Litvak, G. G. Denisov, V. E. Myasnikov, E. M. Tai, E. A. Azizov, and V. I. Ilin, J. Infrared, Millimeter, Terahertz Waves **32**, 337 (2011).

2. M. Thumm, KIT Scientific Report No. 7750 (Karlsruhe Inst. of Technology, 2018).

3. V. E. Zapevalov, Radiophys. Quantum Electron. **49**, 779 (2006).

4. Sh. E. Tsimring, Int. J. Infrared Millimeter Waves **22**, 1433 (2001).

5. N. A. Zavol'skii, V. E. Zapevalov, A. N. Kuftin, and A. S. Postnikova, *Proc. XXVIII Int. Crimean Conf. "Microwave and Telecommunication Technology," Sevastopol, Russia, 2018*, p. 1131.

6. O. I. Louksha, Doctoral Dissertation in Mathematics and Physics (St. Petersburg State Polytechnic Univ., St. Petersburg, 2011).

7. D. V. Kas'yanenko, O. I. Louksha, B. Piosczyk, G. G. Sominsky, and M. Thumm, Radiophys. Quantum Electron. **47**, 414 (2004).

8. O. Louksha, B. Piosczyk, G. Sominski, M. Thumm, and D. Samsonov, IEEE Trans. Plasma Sci. **34**, 502 (2006).

9. O. I. Louksha, D. B. Samsonov, G. G. Sominskii, and A. A. Tsapov, Tech. Phys. **57**, 835 (2012).

10. O. I. Louksha, D. B. Samsonov, G. G. Sominskii, and S. V. Semin, Tech. Phys. **58**, 751 (2013).

11. O. I. Louksha, G. G. Sominski, A. V. Arkhipov, N. V. Dvoretskaya, N. G. Kolmakova, D. B. Samsonov, and P. A. Trofimov, IEEE Trans. Plasma Sci. **44**, 1310 (2016).

12. V. N. Manuilov, M. V. Morozkin, O. I. Luksha, and M. Y. Glyavin, Infrared Phys. Technol. **91**, 46 (2018).

13. H. G. Kosmahl, Proc. IEEE **70**, 1325 (1982).

14. A. L. Goldenberg, V. N. Manuilov, M. A. Moiseev, and N. A. Zavolsky, Int. J. Infrared Millimeter Waves **18**, 43 (1996).

15. A. Singh, S. Rajapatirana, Y. Men, V. L. Granatstein, R. L. Ives, and A. J. Antolak, IEEE Trans. Plasma Sci. **27**, 490 (1999).

16. G. Ling, B. Piosczyk, and M. K. Thumm, IEEE Trans. Plasma Sci. **28**, 606 (2000).

17. M. Y. Glyavin, M. V. Morozkin, and M. I. Petelin, Radiophys. Quantum Electron. **49**, 811 (2006).

18. I. Gr. Pagonakis, J.-P. Hogge, S. Alberti, K. A. Avramides, and J. L. Vomvoridis, IEEE Trans. Plasma Sci. **36**, 469 (2008).

19. O. I. Louksha and P. A. Trofimov, Tech. Phys. Lett. **41**, 884 (2015).

20. C. Wu, I. G. Pagonakis, K. A. Avramidis, G. Gantenbein, S. Illy, M. Thumm, and J. Jelonnek, Phys. Plasmas **25**, 033108 (2018).

21. O. I. Louksha and P. A. Trofimov, *Proc. 41st Int. Conf. Infrared, Millimeter, and Terahertz Waves, Copenhagen, Denmark, 2016*, p. 7758519.
https://doi.org/10.1109/IRMMW-THz.2016.7758519

22. O. I. Louksha and P. A. Trofimov, *Proc. 18th Int. Vacuum Electronics Conf., London, United Kingdom, 2017.*
https://doi.org/10.1109/IVEC.2017.8289518

23. http://www.cst.com.

24. O. I. Louksha and P. A. Trofimov, Tech. Phys. **63**, 598 (2018).

25. E. G. Avdoshin, L. V. Nikolaev, I. N. Platonov, and Sh. E. Tsimring, Radiophys. Quantum Electron. **16**, 461 (1973).

26. J. Zhang, S. Illy, I. Pagonakis, K. A. Avramidis, M. Thumm, and J. Jelonnek, Nucl. Fusion **56**, 026002 (2015).

27. V. N. Manuilov, Radiophys. Quantum Electron. **49**, 786 (2006).

28. O. I. Luksha, Radiophys. Quantum Electron. **52**, 386 (2009).

29. G. P. Saraph, K. L. Felch, J. Feinstein, P. Borchard, S. R. Cauffman, and S. Chu, IEEE Trans. Plasma Sci. **28**, 830 (2000).

30. K. Sakamoto, M. Tsuneoka, A. Kasugai, T. Imai, T. Kariya, K. Hayashi, and Y. Mitsunaka, Phys. Rev. Lett. **73**, 3532 (1994).

31. N. P. Venediktov, M. Yu. Glyavin, V. E. Zapevalov, and A. N. Kuftin, Radiophys. Quantum Electron. **41**, 449 (1998).

32. M. V. Morozkin, M. Y. Glyavin, G. G. Denisov, and A. G. Luchinin, Int. J. Infrared Millimeter Waves **29**, 1004 (2008).

33. B. Piosczyk, C. T. Iatrou, G. Dammertz, and M. Thumm, IEEE Trans. Plasma Sci. **24**, 579 (1996).

Translated by N. Petrov